Title: Synaptopodin is necessary for *Shigella flexneri* intercellular spread.

Authors: Jenna M. Vickery[1], Jody D. Toperzer[1], Julie E. Raab[1], Laurel L. Lenz[1], Sean P. Colgan[2], Brian C. Russo[1*]

1. Department of Immunology and Microbiology, University of Colorado School of Medicine, Aurora, CO 80045, USA

2. Division of Gastroenterology and Hepatology, Department of Medicine, University of Colorado School of Medicine, Aurora, CO 80045, USA

*Corresponding author

Mailing address: 12800 East 19th Avenue, Mail Stop 8333, Aurora, CO 80045, USA

Phone: 303-724-9033

Email: brian.russo@cuanschutz.edu

Abstract

For many intracellular pathogens, their virulence depends on an ability to spread between cells of an epithelial layer. For intercellular spread to occur, these pathogens deform the plasma membrane into a protrusion structure that is engulfed by the neighboring cell. Although the polymerization of actin is essential for spread, how these pathogens manipulate the actin cytoskeleton in a manner that enables protrusion formation is still incompletely understood. Here, we identify the mammalian actin binding protein synaptopodin as required for efficient intercellular spread. Using a model cytosolic pathogen, *Shigella flexneri,* we show that synaptopodin increases actin recruitment around bacteria and stabilizes the position of the actin tail at the posterior pole of the bacteria. We show that synaptopodin presence enables protrusions to form and to resolve at a greater rate, indicating that the proper alignment of the tail enables the bacteria to push against the membrane with greater force. We demonstrate that synaptopodin recruitment around bacteria requires the bacterial protein IcsA, and we show that this recruitment is further enhanced in a type 3 secretion system dependent manner. Myosin X, known to enhance protrusion formation, is associated with more intracellular bacteria in the presence of synaptopodin. These data establish synaptopodin as required for intracellular bacteria to reprogram the actin cytoskeleton in a manner that enables efficient protrusion formation and enhance our understanding of the cellular function of synaptopodin.

Keywords: Synaptopodin; *Shigella flexneri*; cell-to-cell spread; intercellular spread; intracellular pathogens; IcsA; Spa15; plasma membrane; protrusions; type 3 secretion system

42 **Significance**

43 Intercellular spread is essential for many cytosolic dwelling pathogens during their
44 infectious life cycle. Despite knowing the steps required for intercellular spread, relatively
45 little is known about the host-pathogen interactions that enable these steps to occur.
46 Here, we identify a requirement for the actin binding protein synaptopodin during
47 intercellular spread by cytosolic bacteria. We show synaptopodin is necessary for the
48 organization and abundance of actin around bacteria. We also demonstrate synaptopodin
49 is necessary for the formation of plasma membrane structures known as protrusions that
50 are necessary for the movement of these bacteria between cells. Thus, these findings
51 implicate synaptopodin as an important actin-binding protein for the virulence of
52 intracellular pathogens that require the actin cytoskeleton and spread between cells.
53

54 **Introduction**

55 Many cytosolic-dwelling pathogens recruit actin-associated proteins to enable
56 intercellular spread in mammalian cells (1), including *Listeria* spp*., Rickettsia* spp*.,*
57 *Burkholderia* spp*., Mycobacterium marinum, Shigella* spp*.,* and poxviruses. The forces
58 generated from the polymerization of actin enable their intracellular motility and
59 movement between cells (2, 3). In order to polymerize actin, these organisms subvert
60 preexisting mammalian cytoskeletal pathways. Whereas the ability to repurpose the
61 cellular cytoskeleton is critical for virulence, the molecular mechanisms that enable actin
62 motility among these pathogens are still incompletely understood (4-6).

63 Synaptopodin is the founding member of a family of natively unfolded proteins.
64 Approximately 20% of synaptopodin is composed of prolines, which prevent the assembly
65 of most secondary structures (7). Synaptopodin can function as a molecular scaffold that
66 interacts with multiple binding partners, including actin (8, 9). The mechanisms of
67 synaptopodin function remain poorly described. It is implicated in promoting actin fiber
68 formation through recruitment of Nck1 and through interaction with RhoA GTPase (10). It
69 promotes barrier integrity of the intestinal epithelium in response to butyrate by localizing
70 to tight junctions, where it interacts with actin fibers (11). In MDCK cells, synaptopodin
71 promotes cellular extrusion by forming a complex known as a contractomere, which
72 comprises synaptopodin, α-actinin-4, β-catenin, and myosin IIb and generates contractile
73 forces along the cell junction (12). Due to the critical role of actin-binding proteins during
74 infection by cytosolic pathogens, we sought to test whether and how synaptopodin
75 contributes to infection.

76 To examine the role of synaptopodin, we focused on interrogating its function during
77 infection by the model cytosolic pathogen *Shigella flexneri.* This Gram-negative bacterium
78 is a leading cause of bacillary dysentery, a form of bloody diarrhea (6). *S. flexneri* causes
79 disease by invading cells of the colonic epithelium and by spreading between cells in this
80 epithelial layer (13, 14). Cytosolic *S. flexneri* express IcsA at one bacterial pole (15). IcsA
81 binds Neural Wiskott-Aldrich syndrome protein (N-WASP), which then recruits the Actin
82 Related Protein 2/3 complex (Arp2/3) and promotes actin nucleation (16). The
83 polymerization of actin enables the bacteria to move in the cytosol of the cell (17). At the
84 periphery of the cell, some bacteria deform the plasma membrane into a protrusion
85 structure that pushes into the neighboring (recipient) cell (18), where it is actively
86 engulfed. In the recipient cell, these protrusions are resolved into double membrane
87 vacuoles. The bacteria quickly escape the double membrane vacuole into the cytosol,
88 where they can repeat this cycle of intercellular spread (19). Intercellular spread allows
89 the bacterium to access nutrients while evading the immune system, and both the
90 invasion of the colonic epithelium and the spread between cells are essential for
91 pathogenesis (5, 20-23). Defining the molecular mechanisms that promote the
92 intercellular spread of *Shigella* is essential to understand how this organism causes
93 disease.

94 Here, we identify the mammalian protein synaptopodin as required for *S.*
95 *flexneri* intercellular spread by enabling the formation of protrusions. Synaptopodin
96 promotes greater abundance of actin around the bacteria in the cytosol and enables the
97 generation of tail structures with more optimized force vectors for generating protrusions.
98 Synaptopodin is recruited to bacteria in a manner that is dependent on the bacterial

99 protein IcsA, and its recruitment is additionally enhanced by a Spa15-dependent bacterial
100 protein. We show that synaptopodin function likely occurs in a manner distinct from
101 previously described pathways. Together, these data, using *S. flexneri* as a model,
102 identify synaptopodin as a critical cellular component that enables intercellular spread by
103 cytosolic pathogens.

104 **Results**

105 **Synaptopodin is required for efficient intercellular spread by *S. flexneri*.**

106 Since *S. flexneri* requires actin polymerization for intercellular spread (6) and since
107 synaptopodin is an actin-binding protein recently demonstrated to be essential for the
108 function of epithelial actin (11), we hypothesized that synaptopodin may contribute to *S.*
109 *flexneri* intercellular spread in epithelial cells. To test this, a plaque assay was used to
110 compare the efficiency of *S. flexneri* intercellular spread through a monolayer of cells that
111 produce synaptopodin to the efficiency of spread through monolayers that lack
112 synaptopodin. In this assay, the bacteria kill the cells as they spread intercellularly,
113 creating a zone of clearance in the monolayer known as a "plaque". Whereas the number
114 of plaques is a function of the efficiency of bacterial invasion, the area of the plaques is a
115 function of the efficiency of intercellular spread. We measured the area of plaques formed
116 in T84 human colonic adenocarcinoma epithelial (T84) cells and Madin-Darby canine
117 kidney (MDCK) cells that either produced a control shRNA or a shRNA specific to
118 synaptopodin (11, 12). Synaptopodin protein levels are reduced by 80% in the T84 cells
119 (11) and 85% in MDCK cells (Fig. S1A-B). The plaques formed in monolayers of these
120 cells were significantly smaller when synaptopodin was knocked down compared to
121 plaques formed in monolayers of cells producing wild-type levels of synaptopodin (Fig.
122 1A-D).

123 We also compared the ability of *S. flexneri* to spread through monolayers of HeLa
124 cells, which are a model cell line to investigate *S. flexneri* infection. We used HeLa cells
125 producing a control shRNA or one of five synaptopodin-specific shRNAs. We observed

126 that plaques formed in monolayers of HeLa cells producing four of the five synaptopodin
127 specific shRNA were smaller than plaques formed in cells producing the control shRNA
128 (Fig. 1E-F and Fig. S1C-D). The four cell lines displaying reduced plaque size also
129 demonstrated a reduction in synaptopodin protein level as measured by western blot (Fig.
130 S1E-F). Thus, the smaller plaque size observed above was unlikely the result of non-
131 specific effects of an individual shRNA. *S. flexneri* replicated at a similar efficiency in T84,
132 MDCK, and HeLa cells that produced or lacked synaptopodin (Fig. S1G-L), indicating that
133 the reduction in plaque size is not due to differences in bacterial replication. Moreover,
134 since similar results were observed in T84, MDCK, and HeLa cells, these data indicate
135 that the requirement of synaptopodin for *S. flexneri* spread is unlikely to be specific for a
136 particular cell type.

137 We hypothesized that the spread defect observed with *S. flexneri* in synaptopodin
138 knockdown cells would be applicable to other pathogens that nucleate actin. *Listeria*
139 *monocytogenes* is a gram-positive bacterium that, like *Shigella,* requires actin-based
140 motility for intercellular spread (24). We compared the ability of *L. monocytogenes* to
141 spread through a monolayer of HeLa cells producing a control shRNA compared to cells
142 producing a shRNA specific to synaptopodin and used fluorescent microscopy to
143 measure the area of spread. Similar to the results observed with *S. flexneri, L.*
144 *monocytogenes* infection resulted in smaller areas of clearing in synaptopodin knock
145 down cells compared to the control cells (Fig. S2), demonstrating that synaptopodin was
146 required for intercellular spread of *Listeria*. Together, these data show that *S. flexneri*
147 and *L. monocytogenes* require synaptopodin for efficient intercellular spread and that the

148 requirement of synaptopodin may be a general feature of intracellular bacterial pathogens
149 that spread.

150 **Synaptopodin is required for protrusion formation by *S. flexneri***

151 To investigate how synaptopodin contributes to efficient intercellular spread, we
152 focused on aspects of the *S. flexneri* intracellular life cycle that require actin. We assessed
153 the ability of bacteria to form plasma membrane protrusions in HeLa cells producing either
154 a control or a synaptopodin-specific shRNA. We determined the percentage of bacteria
155 present in a protrusion at 90 minutes of infection by examining the manner of actin
156 polymerized at the posterior pole of bacteria by immunofluorescence microscopy. A
157 smaller percentage of bacteria in synaptopodin knockdown cells were present in plasma
158 membrane protrusions compared the percentage of bacteria in protrusions in control cells
159 (Fig. 2A-B), demonstrating that synaptopodin is required for efficient protrusion formation.

160 Synaptopodin is associated with the bundling and elongation of actin filaments in
161 cells (25, 26), but actin intensity at the plasma membrane near protrusions was similar in
162 the presence and absence of synaptopodin (Fig. 2C), indicating that the protrusion defect
163 is not due to defects in the amount of actin recruited to protrusions. Protrusion formation
164 is also dependent on actin that is polymerized by formins. The formin mDia1 is required
165 for formation of protrusions by *S. flexneri* and *Listeria monocytogenes* (27, 28). mDia1
166 was efficiently recruited to protrusions formed in control or synaptopodin knockdown cells
167 (Fig. S3), indicating reduced mDia1 levels around bacteria are not driving the reduction
168 in protrusion formation in the relative absence of synaptopodin. The length of the
169 protrusion is more generally associated with the efficiency of intercellular spread (29).

170 Protrusion lengths were similar irrespective of synaptopodin levels in HeLa cells (Fig. 2D),
171 indicating that the requirement for synaptopodin was not associated with protrusion
172 length.

173 We next investigated the kinetics of protrusion formation by *S. flexneri* to further
174 clarify the role of synaptopodin in the development of membrane protrusions. To visualize
175 the formation of protrusions, intracellular bacteria were tracked by time-lapsed
176 microscopy during infection of HeLa cells that produce a YFP that is anchored to the
177 plasma membrane (30). Bacteria in control cells formed protrusions at a greater velocity
178 than bacteria in cells lacking synaptopodin (Fig. 2E-F). Protrusions formed in the relative
179 absence of synaptopodin were also slower to resolve, lasting an average of 27 min
180 compared to 18 min in controls cells (Fig. 2G). These data show synaptopodin enables
181 more rapid formation and resolution of protrusions.

182 **Synaptopodin regulates actin tail formation by *S. flexneri***

183 The ability to efficiently assemble an actin tail in the cell cytosol is associated with
184 efficient protrusion formation at the plasma membrane (31). We hypothesized that the
185 defects in protrusion formation were the result of aberrant actin tail formation. To test this,
186 we infected HeLa cells with *S. flexneri* and characterized the actin tails. Although a similar
187 percentage of bacteria formed actin tails in the control and synaptopodin knockdown cells
188 (Fig. 3A-B), actin tails that formed in the synaptopodin knockdown cells were visibly
189 different compared to those that formed in the control cells. Actin tails in the control cells
190 were significantly longer than actin tails in the synaptopodin knock down cells (Fig. 3C),
191 and the width of the actin tails at the base of the bacteria was wider in control cells than

192 in synaptopodin knockdown cells (Fig. 3D). In MDCK cells, the actin tails formed in the
193 control cells were also significantly longer than tails in the synaptopodin knockdown cells
194 (Fig. S4A-B). Interestingly, there were no difference observed in the width of the actin tail
195 at the base of the bacteria in MDCK cells (Fig. S4C). Previous studies have shown that
196 the length of the actin tails correlates with the rate of actin polymerization and the speed
197 bacteria move in the cytosol (32). Since we observed shorter tails in HeLa and MDCK
198 cells, it suggested to us that the rate of actin polymerization could be reduced in the
199 absence of synaptopodin and would result in *S. flexneri* moving more slowly through the
200 cytosol of the cells. To test this, time-lapsed microscopy was performed on intracellular
201 bacteria in HeLa cells to evaluate the efficiency of actin-based motility. In contrast to our
202 expectation based on the length of the actin tails, the bacterial velocity was similar in the
203 control and synaptopodin knockdown cells (Fig. 3E-F).

204 In addition to differing in length, polymerized actin was more frequently present
205 along the sides of the posterior end of bacteria in the control cells compared to in
206 synaptopodin knockdown cells (Fig. 3A and G). During bacterial infection or when
207 examining actin polymerization around lipid vesicles, the actin on the sides of the bacteria
208 or vesicle creates an inward force at the base that is predicted to contribute to the
209 propulsive force (33, 34). Seeing that there was no difference in the velocity at which *S.*
210 *flexneri* traveled whether or not actin extended along the sides of the bacteria, we
211 hypothesized that the additional actin may stabilize the tail and keep the actin tail in line
212 with the bacteria, which we anticipated would stabilize the path along which the bacteria
213 travels. To investigate this, we measured the angle at which the actin tail extended from
214 the posterior pole of the bacteria. We set actin tails that formed completely in line with the

215 longitudinal axis of the bacteria at 0° and deviations from this alignment resulted in an
216 increased angle. In the synaptopodin knockdown cells, the actin tails were less aligned
217 with the bacteria's longitudinal axis than the tails associated with bacteria in the control
218 cells, which resulted in a greater angle from the longitudinal axis for bacteria in
219 synaptopodin knockdown cells (Fig. 3H). These data show that synaptopodin enables
220 actin presence along the lateral sides near the posterior end of the bacteria and that
221 synaptopodin enables the actin tail to be more in line with the bacteria. We theorized that
222 the angle of the actin tail would decrease the forward momentum that the actin nucleation
223 creates at the base of the bacteria. We used the formula $[sin\ (angle\ of\ the\ tail(\theta)) +$
224 $cos(angle\ of\ the\ tail(\theta)])$ to calculate the force of the actin tail on the bacteria. We then
225 calculated the percentage of force that contributed to the forward momentum of the
226 bacteria by the formula $[cos\ (angle\ of\ the\ tail(\theta))\ /\ total\ force] * 100$. The percentage
227 of the theoretical forward movement of bacteria in the control cells is higher than in the
228 synaptopodin knockdown cell lines (Fig. 3I). We hypothesized that the defects in the actin
229 tail length, width, organization, and angle of attachment would lead to a defect in the linear
230 trajectory of the bacteria in the absence of synaptopodin. We tracked intracellular bacteria
231 with time-lapsed microscopy to evaluate the linear trajectory. We calculated the distance
232 an individual bacteria traveled and divided it by the distance of the theoretical most
233 efficient path – a straight line. A bacterium that took the most efficient path would have a
234 linear trajectory ratio of 1.0. We observed that bacteria deviated further from an ideal path
235 in cells lacking synaptopodin compared to control cells (Fig. 3E and J), which showed
236 that bacteria traveled along a straighter path in the presence of synaptopodin. These data
237 show that synaptopodin regulates the actin tail around bacteria (Fig. 3K) and contributes

238 to the path the bacteria follow but does not affect the velocity of their actin-based motility
239 in the cytosol.

240 **Synaptopodin colocalizes with actin around *S. flexneri***

241 Based on the requirement for synaptopodin in organizing the actin tail and in
242 forming protrusions, we hypothesized that *S. flexneri* would recruit synaptopodin during
243 intracellular infection. To test this, we infected HeLa and MDCK cells with *S. flexneri* and
244 used immunofluorescence microscopy to visualize synaptopodin localization in cells.
245 Both cell lines showed that synaptopodin was recruited to bacteria in the cytosol (Fig. S5-
246 6). Furthermore, synaptopodin localizes to bacteria that also displayed actin recruitment,
247 but synaptopodin was not observed around bacteria that failed to recruit actin (Fig. S5-
248 6). These data show that synaptopodin is recruited to bacteria that nucleate actin
249 polymerization.

250 Knockdown of synaptopodin caused fewer bacteria to recruit synaptopodin (Fig.
251 S5A-B), and among the bacteria that showed synaptopodin recruitment, there was a
252 reduction in the intensity of synaptopodin (Fig. S5C). Although loss of synaptopodin did
253 not reduce the percent of bacteria that formed an actin tail (Fig. 3B), the knockdown of
254 synaptopodin significantly reduced the number of bacteria that recruited actin (Fig. S5D),
255 yet there was not a significant difference in the intensity of the actin signal among the
256 bacteria that recruited actin in the presence or absence of synaptopodin (Fig. S5E). These
257 data show that synaptopodin is recruited to intracellular bacteria and promotes actin
258 polymerization around bacteria.

259 **Synaptopodin promotes myosin X recruitment around *S. flexneri*.**

260 The localization of IcsA to the posterior pole of *S. flexneri* results in the recruitment
261 of N-WASP and the Arp2/3 complex and enables the initiation of actin polymerization and
262 bacterial motility (16). Synaptopodin is known to regulate this process through another
263 protein Nck1 (35). Synaptopodin promotes Nck1 abundance in cells by blocking c-Cbl-
264 mediated ubiquitination of Nck1, and Nck1 assists in N-WASP and Arp2/3 recruitment
265 during vaccina virus infection (35, 36). We tested whether the defect in actin recruitment
266 in cells lacking synaptopodin was due to a disruption in this synaptopodin-Nck1-Arp2
267 pathway. We observed a similar percentage of bacteria that recruited Arp2, and these
268 bacteria were associated with similar levels of Arp2 as measured by the intensity of the
269 fluorescent signal of Arp2 around bacteria (Fig. S7A-C). We tested whether Nck1 was
270 recruited to the bacteria during intracellular infection. We found no evidence of Nck1
271 recruitment in our cells (Fig. S7D). We examined the ability of *S. flexneri* to recruit N-
272 WASP and observed a similar percentage of bacteria recruited N-WASP (Fig. S7E-F).
273 Among the bacteria that recruited N-WASP, the amount of N-WASP was similar
274 irrespective of synaptopodin levels (Fig. S7G). Together, these data show that
275 synaptopodin facilitates actin organization around the bacteria, but it remains uncertain
276 how synaptopodin alters the organization of actin in our system.

277 We further sought to examine whether we could identify interactions that were
278 important for the formation of the protrusion. Synaptopodin is described to interact with
279 myosin X and α-actinin-4 at the plasma membrane, where together they form the
280 contractomere complex that generates force so as to enable the extrusion of cells from a
281 monolayer (12). Myosin X is required for the formation of protrusions by *S. flexneri* (29),
282 and recent work shows that α-actinin-4 is present at actin structures formed during *S.*

283 *flexneri* infection (1). We tested for the recruitment of myosin X and α-actinin-4 by
284 immunofluorescence microscopy. Interestingly, a smaller percentage of bacteria recruited
285 myosin X in the absence of synaptopodin (Fig. 4A and B), but among the bacteria that
286 recruited myosin X, there was a similar abundance of myosin X as measured by
287 fluorescent intensity irrespective of synaptopodin levels (Fig. 4C). We observed similar
288 levels of α-actinin-4 recruited to bacteria and similar abundance of α-actinin-4 around the
289 bacteria as measured by fluorescent intensity in control and synaptopodin knockdown
290 cells (Fig. 4D-F). Altogether, these data indicate that synaptopodin presence enhances
291 myosin X recruitment around *S. flexneri*.

292 **IcsA and the type 3 secretion system regulate synaptopodin recruitment around *S.***
293 ***flexneri.***

294 *S. flexneri* requires a type three secretion system (T3SS) for intercellular spread (37-39).
295 This type 3 secretion system delivers over 30 bacterial virulence proteins (effectors) into
296 the cell (40). The delivered effectors coopt cellular signaling pathways and enable *S.*
297 *flexneri* to thrive in the intracellular environment. Here, we sought to determine whether
298 synaptopodin was recruited around the bacteria indirectly due to the high concentrations
299 of polymerized actin around the bacteria, as a result of direct recruitment by *S.*
300 *flexneri* secreted proteins, or both. To do so, we tested whether IcsA or the type 3
301 secreted effector proteins contributed to synaptopodin recruitment by investigating
302 synaptopodin localization during cellular infection by several bacterial mutants: *S. flexneri*
303 △*icsA* is unable to polymerize actin; *S. flexneri* △*spa15* lacks a chaperone for nine type 3
304 secreted effector proteins – the absence of Spa15 results in these proteins being unstable

305 and degraded (41); *S. flexneri* △*mxiE* lacks the MxiE transcription factor that is necessary
306 to transcriptionally activate the expression of more than 25 effectors – in the absence of
307 MxiE these effectors are not produced in the bacteria (42-44). Together, the absence of
308 Spa15 and MxiE enabled us to examine whether more than 30 effectors contribute to
309 synaptopodin recruitment as two pooled groups. We infected HeLa cells with these
310 mutants and quantified the percentage of bacteria that showed recruitment of
311 synaptopodin and/or actin, and we measured the intensities of these recruited proteins.
312 As expected, *S. flexneri* △*icsA* did not recruit actin or form actin tails during intracellular
313 infection (Fig. 5A-B). Interestingly, bacteria lacking IcsA also did not recruit synaptopodin
314 (Fig. 5C). A similar percentage of wild-type bacteria and bacteria lacking MxiE recruited
315 actin and synaptopodin (Fig. 5A-C). Loss of Spa15 resulted in a smaller percentage of
316 bacteria that recruited actin compared to wild-type bacteria, but a similar percentage of
317 wild-type and Spa15 deficient bacteria recruited synaptopodin (Fig. 5C). When we
318 examined the amount of actin and synaptopodin recruited around bacteria by comparing
319 the intensity of fluorescent signal, we observed that except for the *icsA* mutant, actin was
320 efficiently recruited around bacteria (Fig. 5D). Yet when we examined the amount of
321 synaptopodin around bacteria, we observed that bacteria lacking Spa15 or IcsA, but not
322 MxiE, recruited less synaptopodin than wildtype bacteria (Fig. 5E). Altogether these data
323 show that bacterial recruitment of synaptopodin is dependent on *S. flexneri* protein IcsA
324 and one or more type 3 secretion system effector proteins regulated by Spa15.

325 **Discussion**

326 Many cytosolic-dwelling pathogens require the subversion of actin and host
327 proteins for intracellular motility. These pathogens remodel the cytoskeleton and plasma
328 membrane resulting in the formation of protrusions, which facilitate intercellular spread.
329 Here, we show that the mammalian protein synaptopodin is recruited to *S. flexneri* in a
330 manner that is dependent on the bacterial protein IcsA and the type 3 secretion system.
331 We show that synaptopodin enables efficient *S. flexneri* intercellular spread by increasing
332 the velocity at which the plasma membrane protrusions form and resolve.

333 Previous studies have shown that the length of the actin tail formed by *Listeria*
334 *monocytogenes* directly correlates with the rate of actin polymerization and the
335 intracellular velocity of the bacteria (32). Although synaptopodin presence enabled longer
336 actin tails to form (Fig. 3C and S4B), synaptopodin loss did not alter the speed the bacteria
337 moved in the cytosol (Fig. 3F). Moreover, proteins associated with actin nucleation, such
338 as N-WASP and Arp2, were efficiently recruited to bacteria irrespective of synaptopodin
339 (Fig. S7A-C and E-G). These findings suggest that rather than altering the rate of actin
340 polymerization, synaptopodin may stabilize the actin filaments that are already formed
341 leading to the generation of longer actin tails. Similar to our findings, the stabilization of
342 F-actin by synaptopodin enables the formation of dendritic spines in neurons (26, 45).
343 Although the tail length did not correlate with bacterial speed in the cytosol, protrusions
344 formed more slowly in the absence of synaptopodin (Fig. 2F). We speculate that this could
345 occur because the rate of addition of new actin monomers as well as the rate of loss of
346 old actin monomers may both contribute to the speed at which the protrusions form.

347 Along with shorter actin tails, bacterial tails formed in the synaptopodin knockdown
348 HeLa cells were less aligned with the longitudinal axis of the bacteria and lacked actin
349 recruitment along the sides of the bacteria. Here, our data indicate that the additional
350 actin provides a stabilizing effect by maintaining actin polymerization in line with the
351 bacterial longitudinal axis and enabling the bacteria to move in a more directed manner
352 forward (Fig. 3J). In MDCK cells, synaptopodin was associated with decreased length of
353 actin tails, but not the width (Fig. S4). Our data indicate that a reduction of actin on the
354 sides of the bacteria does not affect the velocity of cytosolic bacteria (Fig. 3). Rather, we
355 speculate that this specific synaptopodin-dependent localization of actin may be
356 necessary at the membrane where the bacteria experience additional forces during the
357 formation of the protrusion.

358 Previous studies have shown that synaptopodin forms a force-generating complex
359 with α-actinin-4 and myosin X that pulls from the pointed-end toward the barbed-end of
360 the actin filaments. This force generation results in the buckling of actin filaments and
361 pulls on the plasma membrane in a manner that causes cells to extrude from a monolayer
362 (12). One role for synaptopodin could be to function as a force-generating complex that
363 pushes actin filaments into the protrusion structure and enables protrusion formation to
364 be more efficient, but we anticipate this is unlikely to occur during infection. The barbed
365 end of the filaments would be proximal to the bacteria where the incorporation of new
366 actin monomers occurs. Thus, force generation by synaptopodin as described for the
367 contractomere complex would generate a resistive force against protrusion formation by
368 pulling the barbed end of actin back into the cell rather than pushing them out of the cell.
369 Yet, we observe protrusions form faster with synaptopodin (Fig. 2E-G). An intriguing

370 possibility is that synaptopodin, as part of the contractomere complex, is anchored at the
371 plasma membrane and pulls the membrane along the actin filaments toward the bacteria.
372 By pulling membrane into the protrusion, the contractomere complex would both create
373 some slack in the membrane so as to enable the bacteria to more efficiently form the
374 protrusion structure and would provide some mechanism for how the significant amount
375 of plasma membrane is redirected into the protrusion. A second possibility is that the
376 presence of synaptopodin simply stabilizes the actin fibers, as described above, so that
377 the loss of actin monomers is less efficient and the fibers remain longer in the protrusion
378 for a greater period of time, thereby promoting the formation of the protrusion structure.

379 *Shigella* spp., *Listeria* spp., *Rickettsia* spp., *Burkholderia* spp., *Mycobacterium*
380 *marinum,* and pox viruses such as vaccina virus are all examples of pathogens that
381 require actin nucleation for their virulence. Recent studies show that mitochondria use
382 similar mechanisms of motility by generating actin comet tails so as to enable organelle
383 segregation during mitosis (46). Our findings show that synaptopodin is a critical regulator
384 of actin polymerization and organization during *S. flexneri* intercellular spread, and we
385 anticipate that our findings represent a more general role of synaptopodin-dependent
386 regulation of actin dynamics in cells and during infection.

387 **METHODS**:

388 **Bacterial Culture:**
389
390 *S. flexneri* strain 2457T is used in this study, and all mutants are derived from this strain
391 (14). *S. flexneri* strains were cultured in trypticase soy broth (TCS) at 37°C and shaken
392 at 250 rpm. Bacteria were transformed with pROEX-Aqua [Addgene; plasmid #42889,
393 (47)] or pBR322-mCherry for live and fixed microscopy. *L. monocytogenes* strain 10403S
394 is used in this study (48). *L. monocytogenes* strains were cultured in trypticase soy broth
395 (TCS) at 37°C.

396 **Cell Culture:**

397 HeLa cells, MDCK cells (gift of Vivian Tang), and T84 cells were maintained at 37°C in
398 5% CO_2. HeLa and MDCK cells were grown in Dulbecco's modified Eagle's Medium
399 (DMEM) supplemented with 10% fetal bovine serum (FBS). T84 cells were grown in
400 Advance DMEM supplemented with 10% FBS and 1% L-glutamine. The generation of
401 T84 cells producing control or synaptopodin specific shRNA were previously described
402 (11), and the generation of MDCK cells producing control or synaptopodin specific shRNA
403 were previously described (12). HeLa cells producing shRNA targeting synaptopodin
404 were generated using retroviral transduction followed by selection with 5 μg/mL
405 puromycin.

406 **Virus Preparation:**

407 3 million 293T cells were seeded in 100 mm dishes in DMEM supplemented with 10%
408 FBS for 24 hours prior to transduction. Cells were transduced with psPAX2 (Addgene,

409 12260), pVSVg, and either pLKO.5 (SHC216) for control shRNA or a synaptopodin
410 specific shRNA (TRCN0000218429, TRCN0000230911, TRCN0000230913,
411 TRCN0000230912, TRCN0000218782), or pmbYFP (Gift of Hervé Agaisse). Plasmids
412 were transfected into cells using calcium phosphate, which was added dropwise to 293
413 cells, which were then left to incubate at 37°C for 24 hours. The next day, the cells were
414 washed twice, and the media was replaced with fresh DMEM supplemented with 10%
415 FBS. After incubation for an additional 24 hours, the culture supernatant containing the
416 viral particles was collected, passed through a 0.45 µm filter, and stored at -20°C.

417 **Viral Transduction:**

418 3 x 10^5 HeLa cells were seeded in 6-well plates and 2 mL of filtered 293 supernatant
419 containing 4mM polybrene was added to the cells and centrifuged for 2 hours at 1000 *g*
420 at 30°C. Cells then were incubated at 37°C for 48 hours, and the media was replaced
421 with DMEM supplemented 10% FBS and 5 µg/mL puromycin. Resistant cells were
422 expanded. For cells transduced with virus encoding the membrane anchored YFP, cells
423 were sorted at the Flow Cytometry Shared Resource Laboratory in the Department of
424 Immunology and Microbiology to enrich for YFP positive cells.

425 **Plaque Assay:**

426 Cells were seeded at 8 x 10^5 cells per well in 6-well plates. The next day, cells were
427 infected with *S. flexneri* at a multiplicity of infection (MOI) of 0.2 for HeLa cells or a MOI
428 of 20 for MDCK cells and for T84 cells. Bacteria were centrifuged onto cells at 800 *g* for
429 10 minutes and incubated at 37°C in 5% CO_2 for 90 min. Media was replaced with DMEM
430 containing 10% FBS, 25 µg/mL gentamicin, and 0.5% agarose, and the cells were

431 incubated for 48 hours. To visualize plaques, a second overlay was added with 0.7%
432 agarose in DMEM with 10% FBS, 25 µg/mL gentamicin, 0.1% neutral red. Following
433 incubation for at least 4 hours, the plates were imaged with an ImmunoSpot S6 Universal
434 Visible/Fluorescent Analyzer (Cellular Technology Limited). Analysis of the plaque area
435 was performed using a pipeline generated in ImageJ in which images were thresholded
436 to remove background, pixel intensity was converted to a binary, and the images were
437 segmented into objects; objects matching plaques on unmodified images were selected,
438 and their area was quantified, as done previously (38).

439 **Spread Assay by Microscopy:**

440 Cells were seeded at 7 x 10^5 cells per well in 6-well plates onto sterile coverslips. The
441 next day, cells were infected with *Listeria monocytogenes* at a MOI of 15 in PBS. The
442 bacteria were centrifuged onto cells at room temperature at 800 *g* for 10 minutes. The co-
443 culture was incubated at 37°C with 5% CO_2 for 45 mins. Excess bacteria were removed
444 by three successive washes with HBSS. Any remaining extracellular bacteria were killed
445 by incubation in DMEM supplemented with 10% FBS and 25 µg/mL gentamicin. The
446 infection was incubated for an additional 24 or 48 hours and then were fixed with 3.7%
447 paraformaldehyde for at least 20 minutes at room temperature. The cells were
448 permeabilized with 1% triton X-100 in PBS for 30 minutes at room temperature. The cells
449 were washed 5 times with PBS. Cells were stained with phalloidin conjugated to Alexa
450 Flour 750 (Invitrogen A30105) washed with PBS, stained with Hoechst 33342 (Biotech
451 No. 5117), washed twice with PBS, and mounted with Prolong Diamond Antifade
452 Mountant (ThermoFisher, P36930). Images were taken at random. 5 fields of view of

453 infection were analyzed per condition per experiment and area of spread was measured
454 with NIS elements.

455 **Quantification of Intracellular Bacteria:**

456 T84 cells were seeded at 8 X 10^5 cells per well, and HeLa cells and MDCK cells were
457 seeded at 4 X 10^5 cells per well in a 6-well plate. The next day, cells were infected with
458 *S. flexneri* at an MOI of 200. The bacteria were centrifuged onto cells at room temperature
459 at 800 *g* for 10 minutes. The co-culture was incubated at 37°C with 5% CO_2 for 45
460 minutes. Excess bacteria were removed by three successive washes with HBSS. Any
461 remaining extracellular bacteria were killed by incubation in DMEM supplemented with
462 10% FBS and 25 µg/mL gentamicin. The infection was incubated for an additional 1, 2,
463 or 3 hours. The cells were washed three times with HBSS, and then the cells were lysed
464 with 0.02% SDS in HBSS. The cell lysates with intact bacteria were serially diluted in TCS
465 broth and plated onto TCS agar to determine the intracellular CFU.

466 **Western Blots:**

467 SDS-PAGE gels were transferred to nitrocellulose using a Turbo semi dry transfer
468 apparatus (BioRad). For detection of antigen, 1:100 rabbit anti-synaptopodin (Abcam,
469 ab224491) was incubated overnight at 4°C in 5% milk. The next day, blots were incubated
470 with 1:5,000 goat anti-rabbit (Jackson Immuno Research Labs, 111-035-144) for 2 hours
471 at room temperature or 1:10,000 anti-β-actin conjugated to HRP (Sigma A3854) for 1 hour
472 at room temperature. Western blots were developed, and the signal was acquired by a
473 G:Box (Syngene). Band intensity was measured using ImageJ (NIH) with the background
474 subtracted.

475 **Localization of Host Proteins:**

476 HeLa cells or MDCK cells were seeded at 8 X 10^5 cells per well in a 6-well plate and
477 cultured for 24 hours (HeLa) or 48 hours (MDCK). On the day of the infection, media was
478 replaced with DMEM containing 10% FBS and 100 mM IPTG. Cells were infected with
479 designated strains of *S. flexneri* harboring pROEX-Aqua. Bacteria were centrifuged onto
480 cells at 800 *g* for 10 minutes and incubated at 37°C in 5% CO_2. At 45 minutes of infection,
481 cells were washed three times with HBSS, and media was replaced with DMEM
482 containing 10% FBS, 25 µg/mL gentamicin, and 100 mM IPTG. After an additional 45
483 minutes, cells were fixed with 3.7% paraformaldehyde for at least 20 minutes at room
484 temperature. The cells were permeabilized with 1% triton X-100 in PBS for 30 minutes at
485 room temperature. The cells were washed 5 times with PBS and incubated in PBS with
486 10% FBS and 1:100 rabbit anti-synaptopodin (Abcam, ab224491), 1:1000 rabbit anti-N-
487 WASP (Santa Cruz Biotechnology Inc, sc100964), 1:500 rabbit anti-α-actinin-4 (Abcam,
488 ab108198), 1:50 rabbit anti-mDia1 (Abcam, AB129167), 1:500 mouse anti-myosin X
489 (Santa Cruz Biotechnology Inc, sc-376942), or 1:50 goat anti-Arp 2 (Novus Biologicals,
490 NB100-1037) overnight at 4°C. The cells were washed with PBS, incubated with 1:100
491 donkey anti-rabbit conjugated with Alexa Fluor 594 (ThermoFisher, A-21207), goat anti-
492 rabbit conjugated with Alexa Fluor 750 (ThermoFisher, A21039), donkey anti-mouse
493 conjugated with Alexa Fluor 594 (Invitrogen, A32744), or donkey anti-goat conjugated
494 with Alexa Fluor 594 (ThermoFisher, A32758) for 2 hours at room temperature, and
495 washed with PBS. Cells were stained with phalloidin conjugated to Alexa Flour 750
496 (Invitrogen A30105) or Alexa Fluor 647 (Invitrogen, A22287), washed with PBS, stained

497 with Hoechst 33342 (Biotech No. 5117), washed twice with PBS, and mounted with
498 Prolong Diamond Antifade Mountant (ThermoFisher, P36930).

499 **Live Imaging for Speed of Cytosolic Bacteria and of Protrusion Formation:**

500 HeLa cells expressing a membrane-anchored yellow fluorescent protein were seeded at
501 8 X 10^5 cells per well on Ibid 2-well chamber slides (Ibidi, 80286). The next day, media
502 was replaced with DMEM supplemented with 10% FBS and 100 mM IPTG, cells were
503 infected with designated strains of *S. flexneri* harboring the pROEX-Aqua plasmid at an
504 MOI of 400. At 1 hour of infection, cells were washed with HBSS 10 times, and media
505 was replaced with DMEM supplemented with 10% FBS, 25 µg/mL gentamicin, and 100
506 mM IPTG. A time-lapsed Z-stack of images was collected with a Nikon Eclipse Ti-2
507 inverted light microscope at 37°C and 5% CO_2 at 10-second intervals for 10 minutes.
508 Images were deconvolved using a Richardson-Lucy algorithm with 20 iterations and all
509 slices within a stack were collapsed into a single image based upon the maximum
510 intensity of pixels in each slice using NIS elements software. For time-lapsed series, in
511 which some focal drift occurred in the XY position, FIJI plugin: Linear Stack Alignment
512 with SIFT, was used to realign timepoints. NIS elements particle tracking software was
513 used to track in-frame bacteria throughout the video to calculate protrusion velocities.
514 Speed was determined for each bacterium by measuring the distance traveled over the
515 duration of time bacterium was in focus.

516 **Live-cell Imaging Analysis for Protrusions Duration:**

517 HeLa cells expressing a membrane-anchored yellow fluorescent protein were seeded at
518 2 X 10^5 cells per well on Ibidi 8-well chamber slides (Ibidi, 80826). The next day, media

519 was replaced with DMEM and 10% FBS and cells were infected with designated strains
520 of *S. flexneri* expressing mCherry at an MOI of 200. At 1 hour of infection, cells were
521 washed with HBSS 10 times, and media was replaced with DMEM supplemented with
522 10% FBS. A time-lapsed Z-stack of images was taken with a Nikon Eclipse Ti-2 inverted
523 light microscope at 37°C and 5% CO_2 at 5-minute intervals for 2.5 hours to examine
524 protrusion duration. Images were deconvolved using a Richardson-Lucy algorithm with
525 20 iterations and all slices within a stack were collapsed into a single image based upon
526 the maximum intensity of pixels in each slice using NIS elements software. Protrusion
527 duration was measured by quantifying the amount of time the bacteria were in each
528 protrusion stage (49).

529 **Microscopy:**

530 Fluorescent images were acquired on a Nikon Eclipse Ti-2 inverted light microscope
531 equipped with an Orca Fusion BT cMOS camera (Hammamatsu), an IRIS 15 cMOS
532 camera (Photometrics), Semrock Brightline filters, and an Oco stage top incubator
533 chamber that enables regulation of temperature, CO_2, and humidity. NIS elements
534 software (Nikon) was used for image acquisition and analysis. Images were deconvolved
535 using a Richardson-Lucy algorithm with 20 iterations. Microscopic images were pseudo-
536 colored and assembled using Adobe photoshop or FIJI (NIH). Images were collected
537 randomly across the coverslip using an automated imaging pipeline created in NIS
538 elements or the samples were blinded prior to imaging. A minimum of five Z-stacks were
539 collected per coverslip with 0.25 μm step size. To display representative images, all slices
540 within a stack were collapsed into a single image based upon the maximum intensity of
541 pixels in each slice using NIS elements software.

542 **Intensity Analysis:**

543 The signal intensity of random spots of synaptopodin, actin, mDia, Arp2, N-WASP, α-
544 actinin-4 and myosin X around bacteria was measured using NIS elements. Three spots
545 were analyzed at each bacterium, and 5-30 bacteria were measured per condition per
546 experiment, and the average intensity was recorded per experiment.

547 **Statistical Analysis:**

548 Statistical difference between means was analyzed with Graph Pad Prism 9. Statistical
549 difference of two means was determined either by Student's t-test or a paired t-test.
550 Differences between the means of multiple groups was determined either by two-way
551 ANOVA with Sidak *post hoc* test or by one-way ANOVA with a Holm-Sidak's *post hoc* test
552 or a Dunnett's *post hoc* test.
553

554 **Acknowledgements**

555 We would like to thank Vivian Tang, Cammie Lesser, and Hervé Agaisse for reagents.
556 We would like to thank Marcia Goldberg, Cristina Penaranda, Marijke Keestra-Gounder,
557 and the Keestra-Gounder lab for helpful discussions. We would like to thank Tinalyn
558 Kupfer and the CU | AMC ImmunoMicro Flow Cytometry Shared Resource,
559 RRID:SCR_021321, for assistance with cell sorting. This work was funded by K22
560 AI137296, the GI and Liver Innate Immune Program at the University of Colorado, and
561 the University of Colorado start-up funds to BCR. JER was funded by T32 AI052066.

562 **Author Contributions**

563 J.M.V and B.C.R wrote the initial draft of the manuscript. J.M.V, S.P.C., L.L.L., and B.C.R
564 designed experiments. J.M.V, J.D.T, B.C.R, and J.E.R preformed experiments. All
565 authors discussed the results and commented on the manuscript.

566

COMPETING FINANCIAL INTEREST

The authors declare no competing financial interest.

570 **REFERENCES**

571 1. A. S. Dhanda, J. A. Guttman, Localization of host endocytic and actin-associated
572 proteins during *Shigella flexneri* intracellular motility and intercellular spreading.
573 *Anat Rec (Hoboken)* 10.1002/ar.24955 (2022).

574 2. J. M. Stevens, E. E. Galyov, M. P. Stevens, Actin-dependent movement of
575 bacterial pathogens. *Nat Rev Microbiol* **4**, 91-101 (2006).

576 3. G. Hiller, K. Weber, L. Schneider, C. Parajsz, C. Jungwirth, Interaction of
577 assembled progeny pox viruses with the cellular cytoskeleton. *Virology* **98**, 142-
578 153 (1979).

579 4. R. L. Lamason, M. D. Welch, Actin-based motility and cell-to-cell spread of
580 bacterial pathogens. *Curr Opin Microbiol* **35**, 48-57 (2017).

581 5. E. Weddle, H. Agaisse, Principles of intracellular bacterial pathogen spread from
582 cell to cell. *PLoS Pathog* **14**, e1007380 (2018).

583 6. H. Agaisse, Molecular and Cellular Mechanisms of *Shigella flexneri*
584 Dissemination. *Front Cell Infect Microbiol* **6**, 29 (2016).

585 7. P. Mundel *et al.*, Synaptopodin: an actin-associated protein in telencephalic
586 dendrites and renal podocytes. *J Cell Biol* **139**, 193-204 (1997).

587 8. J. M. Chalovich, M. M. Schroeter, Synaptopodin family of natively unfolded, actin
588 binding proteins: physical properties and potential biological functions. *Biophys*
589 *Rev* **2**, 181-189 (2010).

590 9. A. Weins *et al.*, Differentiation- and stress-dependent nuclear cytoplasmic
591 redistribution of myopodin, a novel actin-bundling protein. *J Cell Biol* **155**, 393-
592 404 (2001).

593 10. K. Asanuma *et al.*, Synaptopodin orchestrates actin organization and cell motility
594 via regulation of RhoA signalling. *Nat Cell Biol* **8**, 485-491 (2006).
595 11. R. X. Wang, J. S. Lee, E. L. Campbell, S. P. Colgan, Microbiota-derived butyrate
596 dynamically regulates intestinal homeostasis through regulation of actin-
597 associated protein synaptopodin. *Proc Natl Acad Sci U S A* **117**, 11648-11657
598 (2020).
599 12. T. Morris, E. Sue, C. Geniesse, W. M. Brieher, V. W. Tang, Synaptopodin stress
600 fiber and contractomere at the epithelial junction. *J Cell Biol* **221** (2022).
601 13. T. L. Hale, Genetic basis of virulence in *Shigella* species. *Microbiol Rev* **55**, 206-
602 224 (1991).
603 14. E. H. Labrec, H. Schneider, T. J. Magnani, S. B. Formal, Epithelial Cell
604 Penetration as an Essential Step in the Pathogenesis of Bacillary Dysentery. *J*
605 *Bacteriol* **88**, 1503-1518 (1964).
606 15. M. B. Goldberg, O. Barzu, C. Parsot, P. J. Sansonetti, Unipolar localization and
607 ATPase activity of IcsA, a *Shigella flexneri* protein involved in intracellular
608 movement. *Infect Agents Dis* **2**, 210-211 (1993).
609 16. C. Egile *et al.*, Activation of the CDC42 effector N-WASP by the *Shigella flexneri*
610 IcsA protein promotes actin nucleation by Arp2/3 complex and bacterial actin-
611 based motility. *J Cell Biol* **146**, 1319-1332 (1999).
612 17. M. L. Bernardini, J. Mounier, H. d'Hauteville, M. Coquis-Rondon, P. J. Sansonetti,
613 Identification of icsA, a plasmid locus of *Shigella flexneri* that governs bacterial
614 intra- and intercellular spread through interaction with F-actin. *Proc Natl Acad Sci*
615 *U S A* **86**, 3867-3871 (1989).

616 18. J. L. Kadurugamuwa, M. Rohde, J. Wehland, K. N. Timmis, Intercellular spread
617 of *Shigella flexneri* through a monolayer mediated by membranous protrusions
618 and associated with reorganization of the cytoskeletal protein vinculin. *Infect*
619 *Immun* **59**, 3463-3471 (1991).
620 19. F. X. Campbell-Valois, M. Sachse, P. J. Sansonetti, C. Parsot, Escape of Actively
621 Secreting *Shigella flexneri* from ATG8/LC3-Positive Vacuoles Formed during
622 Cell-To-Cell Spread Is Facilitated by IcsB and VirA. *mBio* **6**, e02567-02514
623 (2015).
624 20. P. J. Sansonetti, J. Arondel, A. Fontaine, H. d'Hauteville, M. L. Bernardini, OmpB
625 (osmo-regulation) and icsA (cell-to-cell spread) mutants of *Shigella flexneri*:
626 vaccine candidates and probes to study the pathogenesis of shigellosis. *Vaccine*
627 **9**, 416-422 (1991).
628 21. T. Suzuki, C. Sasakawa, Molecular basis of the intracellular spreading of
629 *Shigella*. *Infect Immun* **69**, 5959-5966 (2001).
630 22. L. K. Yum, M. X. Byndloss, S. H. Feldman, H. Agaisse, Critical role of bacterial
631 dissemination in an infant rabbit model of bacillary dysentery. *Nat Commun* **10**,
632 1826 (2019).
633 23. P. S. Mitchell *et al.*, NAIP-NLRC4-deficient mice are susceptible to shigellosis.
634 *Elife* **9** (2020).
635 24. J. R. Robbins *et al.*, *Listeria monocytogenes* exploits normal host cell processes
636 to spread from cell to cell. *J Cell Biol* **146**, 1333-1350 (1999).
637 25. K. Ichimura, H. Kurihara, T. Sakai, Actin filament organization of foot processes
638 in rat podocytes. *J Histochem Cytochem* **51**, 1589-1600 (2003).

639 26. K. Yap *et al.*, The actin-modulating protein synaptopodin mediates long-term
640 survival of dendritic spines. *Elife* **9** (2020).
641 27. J. E. Heindl, I. Saran, C. R. Yi, C. F. Lesser, M. B. Goldberg, Requirement for
642 formin-induced actin polymerization during spread of *Shigella flexneri*. *Infect*
643 *Immun* **78**, 193-203 (2010).
644 28. R. Fattouh *et al.*, The diaphanous-related formins promote protrusion formation
645 and cell-to-cell spread of *Listeria monocytogenes*. *J Infect Dis* **211**, 1185-1195
646 (2015).
647 29. E. A. Bishai *et al.*, Myosin-X facilitates *Shigella*-induced membrane protrusions
648 and cell-to-cell spread. *Cell Microbiol* **15**, 353-367 (2013).
649 30. A. M. Dragoi, H. Agaisse, The serine/threonine kinase STK11 promotes *Shigella*
650 *flexneri* dissemination through establishment of cell-cell contacts competent for
651 tyrosine kinase signaling. *Infect Immun* **82**, 4447-4457 (2014).
652 31. D. M. Monack, J. A. Theriot, Actin-based motility is sufficient for bacterial
653 membrane protrusion formation and host cell uptake. *Cell Microbiol* **3**, 633-647
654 (2001).
655 32. J. A. Theriot, T. J. Mitchison, L. G. Tilney, D. A. Portnoy, The rate of actin-based
656 motility of intracellular *Listeria monocytogenes* equals the rate of actin
657 polymerization. *Nature* **357**, 257-260 (1992).
658 33. F. Gerbal, P. Chaikin, Y. Rabin, J. Prost, An elastic analysis of *Listeria*
659 *monocytogenes* propulsion. *Biophys J* **79**, 2259-2275 (2000).

660 34. P. A. Giardini, D. A. Fletcher, J. A. Theriot, Compression forces generated by
661 actin comet tails on lipid vesicles. *Proc Natl Acad Sci U S A* **100**, 6493-6498
662 (2003).
663 35. L. Buvall *et al.*, Proteasomal degradation of Nck1 but not Nck2 regulates RhoA
664 activation and actin dynamics. *Nat Commun* **4**, 2863 (2013).
665 36. V. Moreau *et al.*, A complex of N-WASP and WIP integrates signalling cascades
666 that lead to actin polymerization. *Nat Cell Biol* **2**, 441-448 (2000).
667 37. R. Schuch, R. C. Sandlin, A. T. Maurelli, A system for identifying post-invasion
668 functions of invasion genes: requirements for the Mxi-Spa type III secretion
669 pathway of *Shigella flexneri* in intercellular dissemination. *Mol Microbiol* **34**, 675-
670 689 (1999).
671 38. J. K. Duncan-Lowey, A. L. Wiscovitch, T. E. Wood, M. B. Goldberg, B. C. Russo,
672 *Shigella flexneri* Disruption of Cellular Tension Promotes Intercellular Spread.
673 *Cell Rep* **33**, 108409 (2020).
674 39. C. J. Kuehl, A. M. Dragoi, H. Agaisse, The *Shigella flexneri* type 3 secretion
675 system is required for tyrosine kinase-dependent protrusion resolution, and
676 vacuole escape during bacterial dissemination. *PLoS One* **9**, e112738 (2014).
677 40. A. Nasser, M. Mosadegh, T. Azimi, A. Shariati, Molecular mechanisms of
678 *Shigella* effector proteins: a common pathogen among diarrheic pediatric
679 population. *Mol Cell Pediatr* **9**, 12 (2022).
680 41. N. H. Ernst, A. Z. Reeves, J. E. Ramseyer, C. F. Lesser, High-Throughput
681 Screening of Type III Secretion Determinants Reveals a Major Chaperone-
682 Independent Pathway. *mBio* **9** (2018).

683 42. T. L. Gall *et al.*, Analysis of virulence plasmid gene expression defines three
684 classes of effectors in the type III secretion system of *Shigella flexneri*.
685 *Microbiology (Reading)* **151**, 951-962 (2005).
686 43. C. D. Kane, R. Schuch, W. A. Day, Jr., A. T. Maurelli, MxiE regulates intracellular
687 expression of factors secreted by the *Shigella flexneri* 2a type III secretion
688 system. *J Bacteriol* **184**, 4409-4419 (2002).
689 44. C. P. Hall, N. B. Jadeja, N. Sebeck, H. Agaisse, Characterization of MxiE- and H-
690 NS-Dependent Expression of ipaH7.8, ospC1, yccE, and yfdF in *Shigella flexneri*.
691 *mSphere* **7**, e0048522 (2022).
692 45. A. Vlachos *et al.*, Synaptopodin regulates plasticity of dendritic spines in
693 hippocampal neurons. *J Neurosci* **29**, 1017-1033 (2009).
694 46. A. S. Moore *et al.*, Actin cables and comet tails organize mitochondrial networks
695 in mitosis. *Nature* **591**, 659-664 (2021).
696 47. M. Erard *et al.*, Minimum set of mutations needed to optimize cyan fluorescent
697 proteins for live cell imaging. *Mol Biosyst* **9**, 258-267 (2013).
698 48. E. M. Eshleman, N. Bortell, D. S. McDermott, W. J. Crisler, L. L. Lenz, Myeloid
699 cell responsiveness to interferon-gamma is sufficient for initial resistance to
700 Listeria monocytogenes. *Curr Res Immunol* **1**, 1-9 (2020).
701 49. E. A. Weddle, V. K. Koseoglu, B. A. DeVasure, H. F. Agaisse, The type three
702 secretion system effector protein IpgB1 promotes *Shigella flexneri* cell-to-cell
703 spread through double-membrane vacuole escape. *PLoS Pathog* **18**, e1010380
704 (2022).
705

706 **FIGURES**

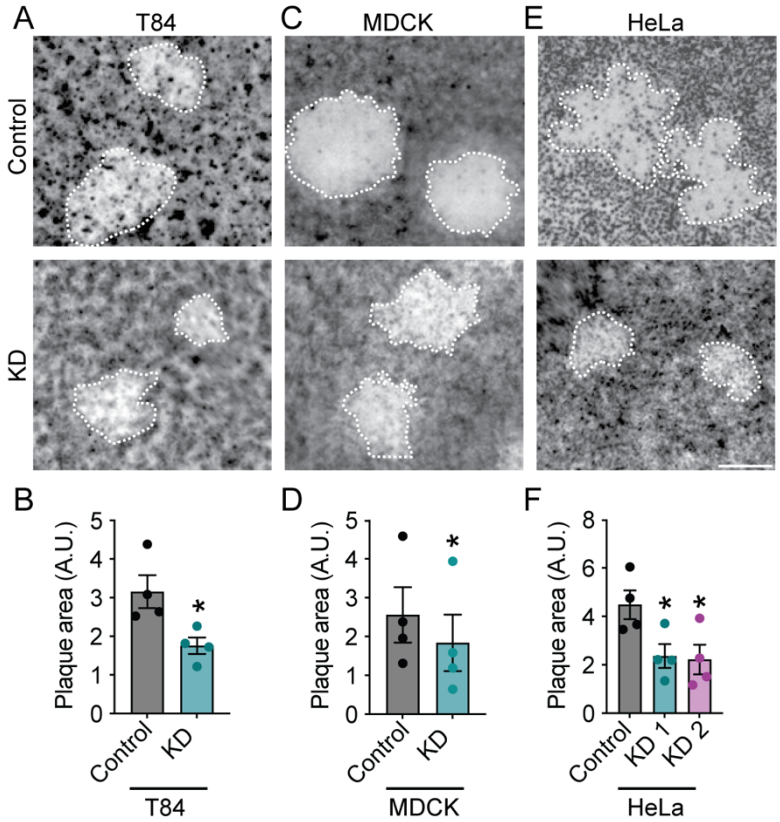

707

708 **Figure 1: Synaptopodin is required for efficient intercellular spread of *S. flexneri***

709 Monolayers of T84 (A-B), MDCK (C-D), or HeLa (E-F) cells that produce a control or
710 synaptopodin specific shRNA were infected with *S. flexneri* and stained with neutral red
711 at 48 hours of infection. (A, C, and E) Representative images. Dotted lines indicate plaque
712 boundary. Scale bar, 0.5 mm. (B, D, and F) Quantification of the area of plaques from
713 images represented in A, C, and E. 15-60 plaques measured per condition per
714 experiment. Dots are independent experiments. *, $p<0.05$ by paired t-test (B and D) or by
715 one-way Dunnett's *post hoc* test (F). Data are mean ± SEM.

716

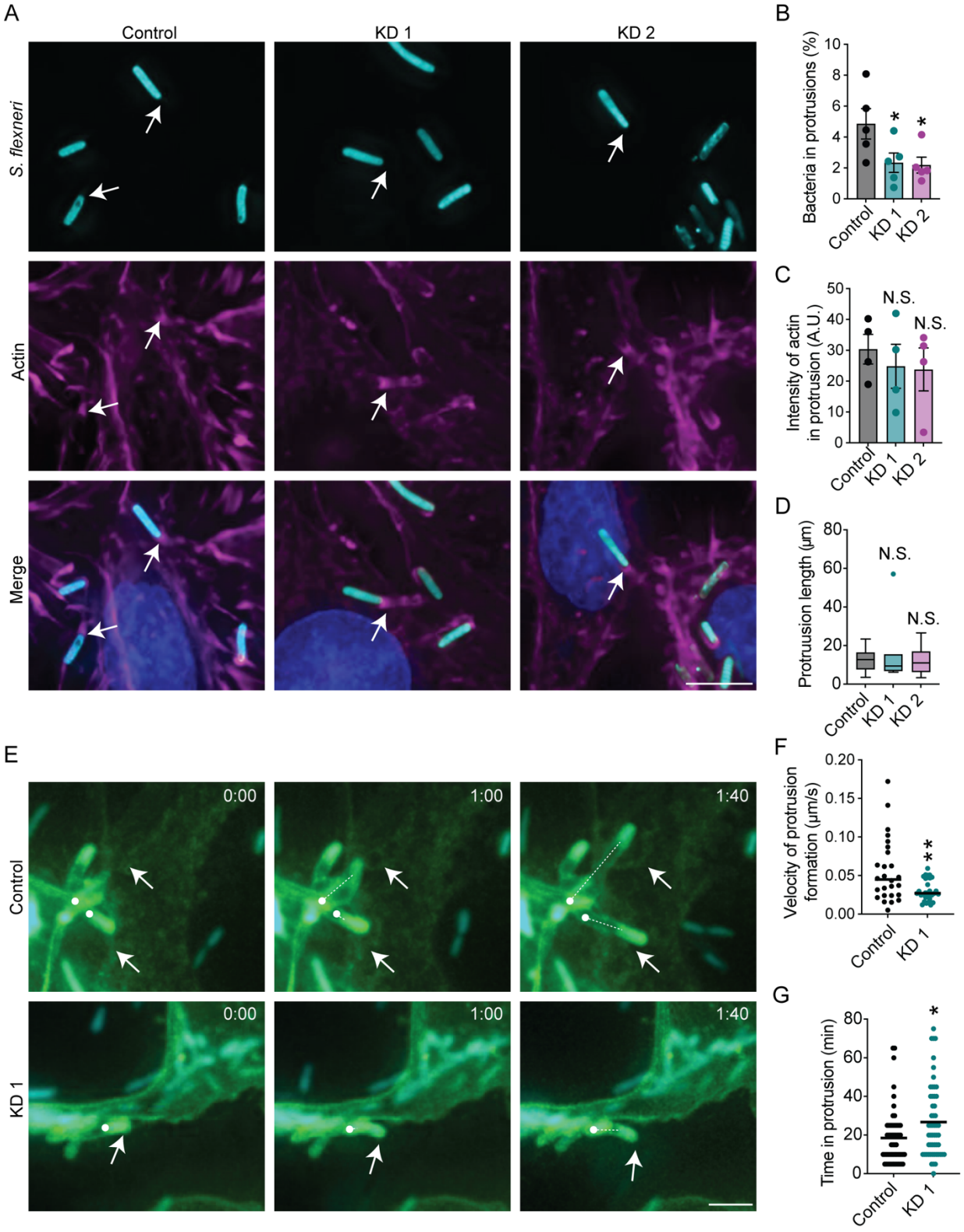

717

718 **Figure 2: Synaptopodin is required for protrusion formation by *S. flexneri***

719 (A) Representative images of HeLa cells infected with *S. flexneri.* Cyan, *S. flexneri;*
720 magenta, actin; blue, DNA. Arrows, bacteria in protrusions. Scale bar, 5 μM. 5-10 fields
721 were analyzed per condition per experiment. (B) Quantification of the percentage of
722 intracellular bacteria within a protrusion. (C) Quantification of the intensity of actin in
723 protrusions. (B and C) Dots are independent experiments. (D) Quantification of the length
724 of protrusions. Tukey method used to define whiskers. (B-D) N.S., not significant; *,
725 $p<0.05$ by one-way ANOVA with Holm-Sidak's *post hoc* test. (E-G) Time lapse images
726 videos of bacteria forming plasma membrane protrusions. (E) Representative images of
727 protrusion formation. Cyan, S. *flexneri;* green, plasma membrane. Scale bar 5 μM.
728 Arrows, bacteria in protrusions; dot, protrusion origination point; dotted line, progression
729 of protrusion formation. (F) Quantification of the speed of protrusion formation from videos
730 represented in E. (G) Quantification of the duration bacteria remain in protrusions. (F-G)
731 Dots are individual bacteria, pooled from 3 independent experiments. *, $p<0.05$ by
732 Student's t-test. Data are mean ± SEM.

733

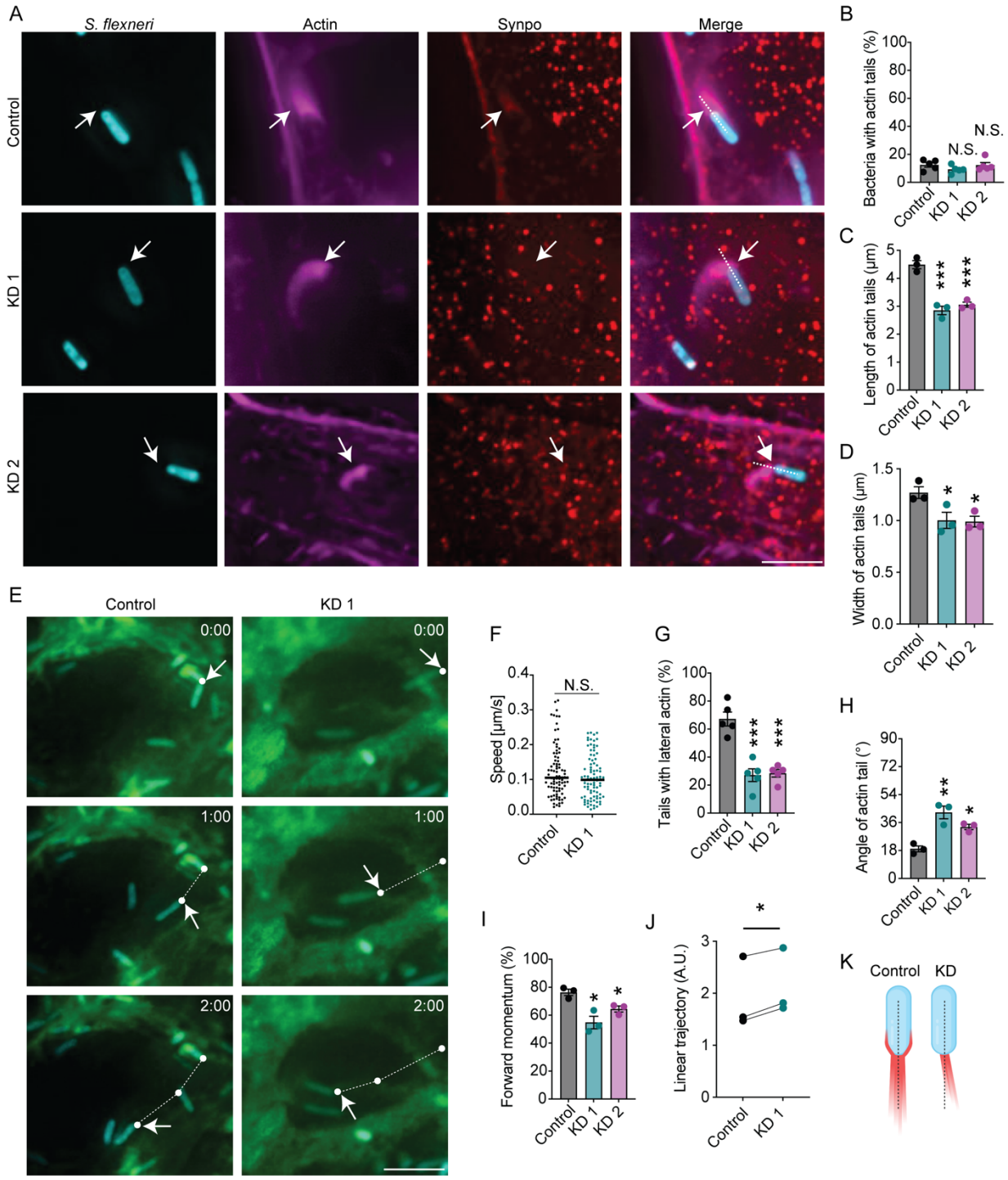

Figure 3: Synaptopodin regulates actin tail formation by *S. flexneri*

736 Infection of HeLa cells infected with *S. flexneri* for 90 min. (A) Representative images.
737 Cyan, *S. flexneri;* magenta, actin; red, synaptopodin; blue, DNA. Arrows, bacteria with
738 actin tails. Scale bar, 5 μM. (B) Quantification of percentage of bacteria with actin tails.
739 (C) Quantification of the length of actin tails. (D) Quantification of the width of actin tails
740 proximal to the bacterial pole. (E-F) Time-lapsed microscopy of HeLa cells producing a
741 membrane anchored YFP infected with *S. flexneri* producing CFP. (E) Representative still
742 images from time-lapsed videos for 2 minutes from initial observation of motility. Cyan, *S.*
743 *flexneri*; green, plasma membrane. Dots are the position of bacteria at each time point,
744 dotted line is arbitrary straight line between dots showing bacterial progression over time.
745 Scale bar, 5 μM. (F) Quantification of the speed at which bacteria move in the cytosol
746 from videos represented in E. Mean indicated by bar. (G) Quantification of the percent of
747 bacteria with an actin tail that also display lateral actin from images represented in A. (H)
748 Quantification of the angle (0°-90°) at which the actin tail is anchored to the bacterial pole
749 with respect to the longitudinal midline of the bacteria from images represented in A. (I)
750 Mathematical estimation of the forward momentum as a result of the angle of the tail from
751 images of bacteria represented in A. 100% forward moment corresponds to a tail angle
752 of 0°. (J) Quantification of the linearity of the path bacteria traveled in the cell from videos
753 represented in E. (K) Schematic of actin tail for bacteria in control or synaptopodin
754 knockdown cells. Created with biorender.com. (B, C, D, G, H, and I) 5-10 fields were
755 analyzed per experiment. Dots are independent experiments. Data are mean ± SEM.
756 N.S., not significant; *, $p<0.05$; **, $p<0.1$; ***, $p<0.001$ by one-way ANOVA with Dunnett's
757 *post hoc* test. (F and J) N.S., not significant; *, $p<0.05$ by Student's t-test (F) or paired t-

758 test (J). Dots are individual bacteria pooled together from three experiments (F) or means

759 of individual experiments (J).

760

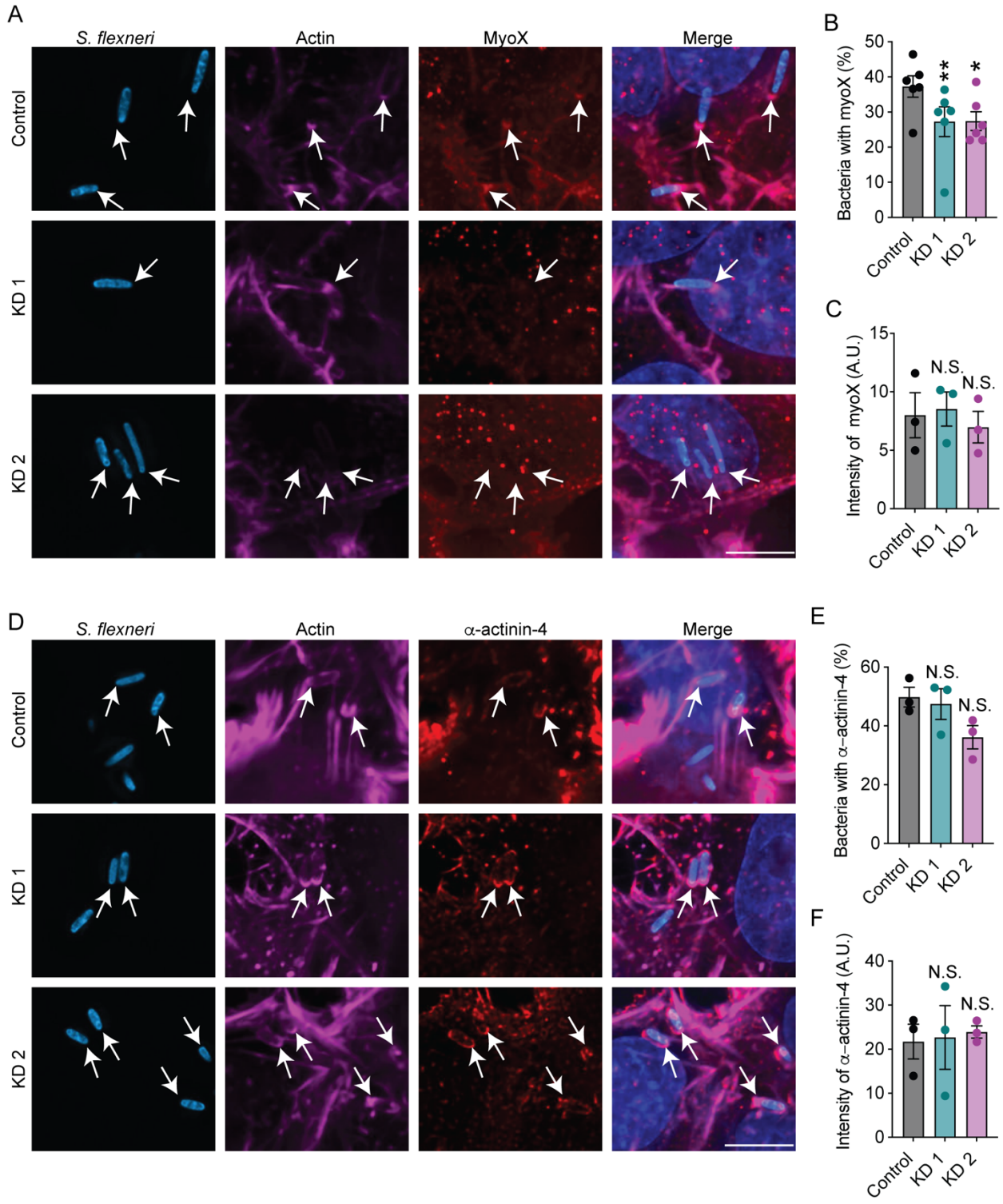

761

762 **Figure 4: Synaptopodin is required for Myosin X recruitment around bacteria**

763 HeLa cells were infected with *S. flexneri* for 90 min. (A) Representative images. Cyan, *S.*
764 *flexneri*; magenta, actin; red, myosin X; blue, DNA. Arrows, bacteria with myosin X. Scale
765 bar, 5 μM. (B) Quantification of percentage of bacteria with myosin X. (C) Quantification
766 of the intensity of myosin X around bacteria. (D) Representative images depicting α-
767 actinin-4 recruitment around bacteria. Cyan, *S. flexneri;* magenta, actin; red, α-actinin-4;
768 blue, DNA. Arrows, bacteria with α-actinin-4. Scale bar, 5 μM. (E) Quantification of the
769 percentage of bacteria with α-actinin-4. (F) Quantification of the intensity of α-actinin-4.
770 (B-C and E-F) 5-10 fields were analyzed per condition per experiment. Dots are
771 independent experiments. Data are mean ± SEM. NS, not significant; *, $p<0.05$; **, $p<0.01$
772 by one-way ANOVA with Dunnett's *post hoc* test.

773

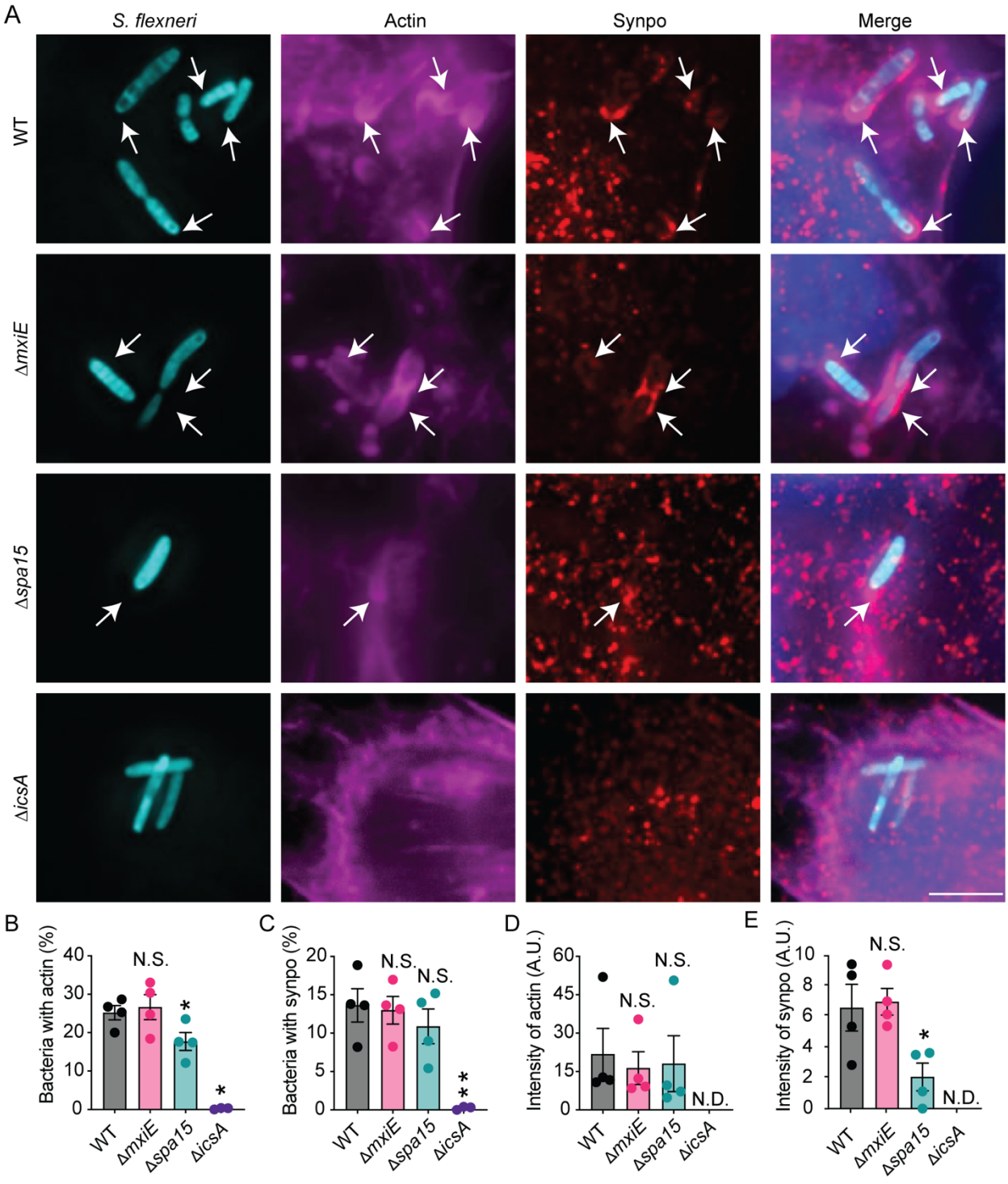

774

775 **Figure 5: Synaptopodin is recruited around *S. flexneri* in an IcsA and a type 3**

776 **secretion system dependent manner**

777 Control HeLa cells were infected for 90 min with *S. flexneri* strains. (A) Representative
778 images. Cyan, *S. flexneri*; magenta, actin; red, synaptopodin (synpo); blue, DNA. Arrows,
779 bacteria with actin and synaptopodin. Scale bar 5 μM. (B) Quantification of the percentage
780 of bacteria with actin. (C) Quantification of the percentage of bacteria with synaptopodin.
781 (D) Quantification of the intensity of actin around bacteria. (E) Quantification of intensity
782 of synaptopodin around bacteria. (B-E) 5-10 fields were analyzed per condition per
783 experiment. Dots are independent experiments. Data are mean ± SEM. N.D., not
784 detected. NS, not significant; *, $p<0.05$; **, $p<0.01$ by one-way ANOVA with Dunnett's
785 *post hoc* test.

786

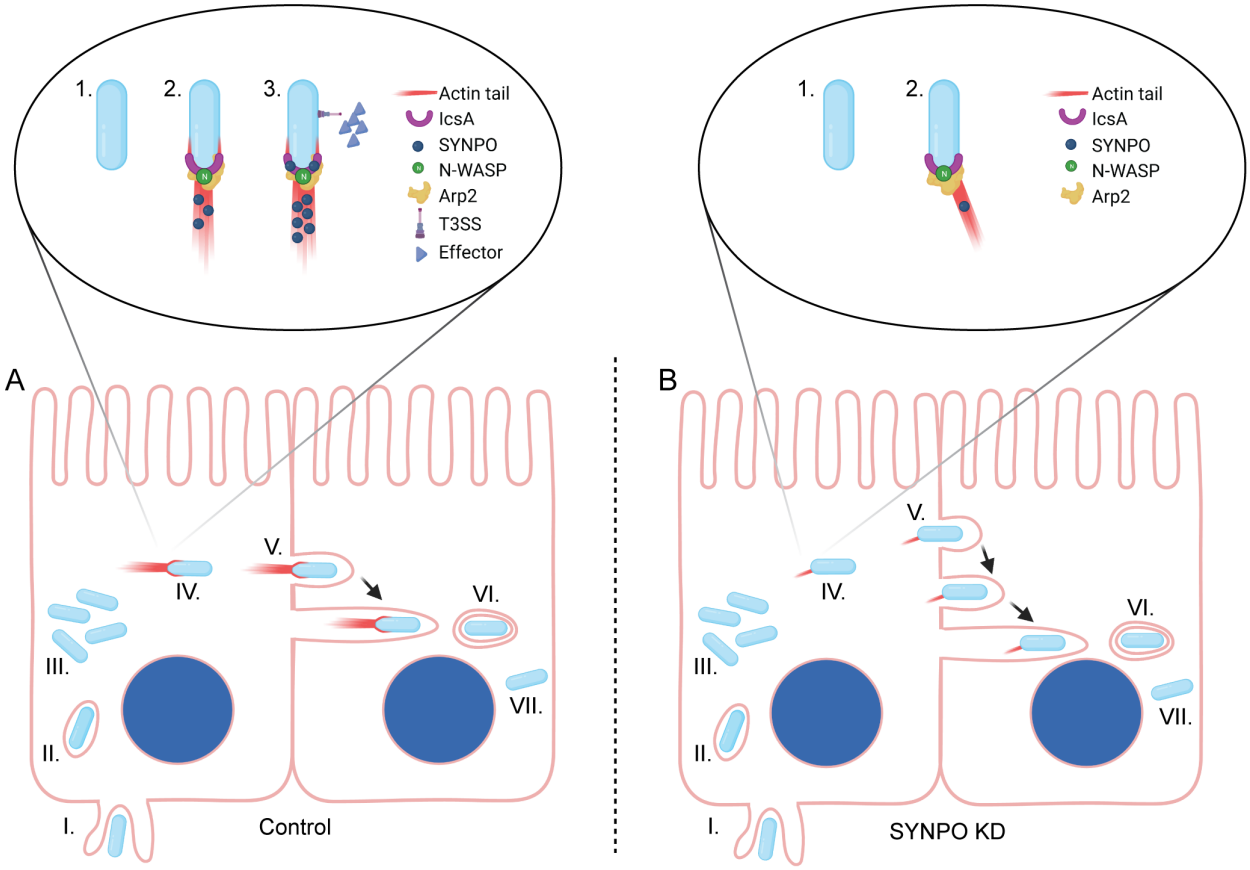

Fig. 6. Schematic of *S. flexneri* intercellular spread in control versus synaptopodin knockdown cell lines.

Schematic of *S. flexneri* intercellular lifecycle. (I) *S. flexneri* induces its uptake into cells. (II) Following uptake, it is present in a vacuole. (III) It escapes the vacuole into the cytosol where the bacteria replicate. (IV) A portion of the bacteria nucleate the polymerization of actin, which enables the bacteria to move in the cell cytosol. (V) Bacteria near the cell periphery deform the plasma membrane into a protrusion. (VI) The protrusion resolves into a double membrane vacuole. (VII) The bacteria escape the double membrane vacuole into the cytosol. (A) Cells with synaptopodin enabled bacteria to form actin tails that are longer and more aligned with the bacteria than cells lacking synaptopodin (IV).

798 Bacteria in cells with synaptopodin form protrusions at a higher velocity that resolve
799 quickly (V). (B) In cells lacking synaptopodin, the actin tails are shorter and less aligned
800 with the bacteria (IV). Protrusions are formed at a slower velocity and take longer to
801 resolve into a double membrane vacuole (V). (A-B) 1. Bacteria lacking IcsA do not
802 polymerize actin or recruit synaptopodin. 2. Polar localization of IcsA is associated with
803 synaptopodin recruitment, and IcsA recruits N-WASP and Apr2/3 irrespective of
804 synaptopodin abundance in cells. 3. Synaptopodin recruitment to bacteria is further
805 enhanced in a type 3 secretion dependent manner. Created with biorender.com